Dalton Transactions

COMMUNICATION

View Article Online
View Journal | View Issue

Cite this: *Dalton Trans.*, 2016, **45**, 7559

Received 29th December 2015,
Accepted 30th March 2016

DOI: 10.1039/c5dt05045f

www.rsc.org/dalton

High methane storage and working capacities in a NbO-type metal–organic framework†

Chengling Song,[a] Huimin Liu,[a] Jingjing Jiao,[a] Dongjie Bai,[a] Wei Zhou,[b] Taner Yildirim[b,c] and Yabing He*[a]

To improve methane adsorption by pore structure optimization, we developed a new organic linker and used it to construct a NbO-type metal–organic framework ZJNU-53 that, after activation, exhibits exceptionally high methane storage and working capacities of 241 and 190 cm^3 (STP) cm^{-3} at 298 K and 65 bar, respectively, if the packing loss is not considered, which are among the highest reported for MOF materials.

Natural gas (NG) is becoming an attractive alternative fuel to gasoline and diesel due to a dramatic increase in the accessibility of shale gas reserves, together with the potential for reduced carbon emissions. However, the low volumetric energy density of methane gas, the primary component of NG, under standard conditions presents a barrier to the widespread adoption of NG as a vehicular fuel. Currently, most natural gas vehicles (NGV) are powered by compressed natural gas (CNG), but the operation cost and safety issues due to the high pressure involved are limiting factors. To overcome these drawbacks associated with compression storage technologies, adsorption technologies using porous materials may offer an appealing option since moderately high-density methane storage can be achieved under relatively mild conditions, *viz.*, ambient temperature and moderate pressure, thus minimizing the efficiency losses. However, the key to the success of adsorbed natural gas (ANG) lies in the development of a suitable adsorbent that can store NG at sufficiently high densities to meet specific driving range requirements. In this regard, porous metal–organic frameworks (MOFs) assembled from the modular combination of inorganic and organic building blocks are considered as good candidates due to their tuneable pore sizes and modifiable pore surfaces suitable for gas adsorption.[1]

The early investigations concerning methane storage on MOFs have mainly concentrated on the improvement of methane storage amount,[2] and some MOFs have been identified as promising materials for methane storage.[2g,3] Although some of them have exhibited relatively high methane storage capacities, the methane deliverable amounts are still limited. For example, NiMOF-74 has the third high volumetric methane uptake of 251 cm^3 (STP) cm^3 at 298 K and 65 bar; however, the deliverable amount of methane is only 129 cm^3 (STP) cm^{-3}, about a half of the total uptake.[3b] For practical application, the methane deliverable amount is more important than the methane storage amount because it determines the driving range of NGVs. Therefore, in the research and development of methane adsorbents, researchers should not only pursue high methane storage amounts of MOF materials, but more importantly should pay much attention to their methane working capacities. However, due to a variety of structural factors influencing the methane adsorption performance, how to design the MOF materials with high methane working capacities has become a long-standing challenge that has triggered tremendous studies to improve the methane working capacities of MOF materials.

Recently, we employed a strategy of inserting a slim C≡C triple bond into a NbO-type MOF NOTT-101 to achieve a MOF material **ZJNU-50a** (thereafter, the letter "a" indicates activated MOF materials) with relatively high methane working capacities of 184 cm^3 (STP) cm^{-3} when the pressures swing from 65 to 5 bar at 298 K.[4] In order to further improve the methane storage performance by means of optimizing the pore structure, we developed a new organic linker H_4L, 5,5′-(naphthalene-1,4-diyl-ethyne-1,2-diyl)diisophthalic acid as shown in Scheme 1, and constructed the corresponding copper-based MOF termed **ZJNU-53**, which is based on the following considerations. (1) In order to obtain high methane deliverable amounts, we need to maximize the methane

[a]*College of Chemistry and Life Sciences, Zhejiang Normal University, Jinhua 321004, China. E-mail: heyabing@zjnu.cn*
[b]*NIST Center for Neutron Research, Gaithersburg, Maryland 20899-6102, USA*
[c]*Department of Materials Science and Engineering, University of Pennsylvania, Philadelphia, Pennsylvania 19104-6272, USA*

† Electronic supplementary information (ESI) available: Synthesis and characterization of the organic linker and **ZJNU-53**, PXRD (Fig. S1), TGA (Fig. S2), BET plot (Fig. S3), pore size distribution (Fig. S4), excess methane adsorption isotherms (Fig. S5), FTIR (Fig. S6), ^{1}H and ^{13}C NMR of the organic linker H_4L in DMSO-d_6 (Fig. S7), ^{1}H NMR spectra of the acid-digested sample in DMSO-d_6 (Fig. S8), crystal data and structure refinement for **ZJNU-53** (Table S1). CCDC 1458075. For ESI and crystallographic data in CIF or other electronic format see DOI: 10.1039/c5dt05045f

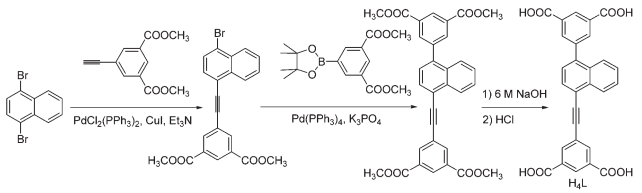

Scheme 1 Synthesis of the organic linker H_4L used to construct **ZJNU-53**.

storage capacities at 65 bar and at the same time minimize methane uptake at a low pressure of 5 bar. To achieve this aim, the replacement of a benzene ring spacer in the organic linker used to construct **ZJNU-50** with a naphthalene ring is expected to increase more methane uptake at a high pressure of 65 bar than that at a low pressure of 5 bar by reducing pore size *via* dissecting the large cages into small ones and by enhancing the gas-framework interactions *via* the polarized π-electron. (2) To our knowledge, no study based on this unsymmetrical organic linker has been reported. Gas adsorption studies showed that compared to the parent compound **ZJNU-50a**, the resulting MOF material, after activation, does indeed show much higher volumetric methane storage and working capacities. Herein, we wish to report the synthesis, characterization, and methane adsorption properties of this MOF material.

The organic linker H_4L was synthesized by subsequent Sonogashira and Suzuki coupling reactions followed by hydrolysis and acidification (Scheme 1). The chemical structures of the organic linker and the corresponding intermediates were characterized unambiguously by ^{1}H NMR and ^{13}C NMR spectroscopy. A solvothermal reaction between the tetracarboxylic acid and $Cu(NO_3)_2{\cdot}3H_2O$ in a mixed solvent of *N*,*N*-dimethylformamide (DMF), methanol and H_2O under acidic conditions at 353 K afforded a crystalline material of **ZJNU-53** in a good yield. The structure was determined by single-crystal X-ray crystallography and the phase purity was confirmed by powder X-ray diffraction studies (Fig. S1 in the ESI†). Based on the single-crystal X-ray diffraction studies, thermogravimetric analysis (TGA, Fig. S2†) and microanalysis, **ZJNU-53** can be best formulated as $[Cu_2L(H_2O)_2]{\cdot}6DMF{\cdot}2H_2O$. The TGA shows a weight loss of 45.8% up to 498 K, corresponding to the loss of free solvents and terminal water molecules ($6DMF + 4H_2O$).

Single-crystal X-ray diffraction studies reveal that **ZJNU-53** crystallizes in a trigonal space group $R\bar{3}m$. The copper ion is coordinated by five oxygen atoms from four carboxylate groups of four different ligands and one terminal water molecule occupying the axial positions, with a Cu–Cu distance of 2.663 Å. A pair of copper centres are linked by four carboxylates to form a paddlewheel secondary building unit (SBU) serving as a 4-connected square-planar node, which are bridged by the 4-connected rectangular organic building blocks to form a three-dimensional (3D) noninterpenetrated 4,4-connected NbO-type network with a Schläfli topological symbol of $\{6^4{\cdot}8^2\}$.[5] In the resulting framework, there are two

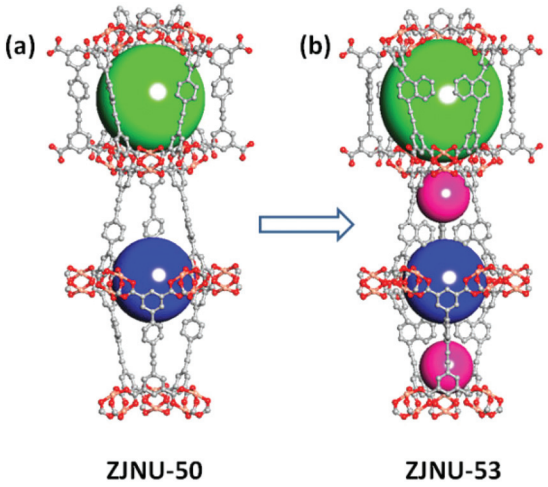

Fig. 1 Single-crystal X-ray structure showing one plausible way of the shuttle-shaped cage partition upon ligand modification.

different types of nanocages which are connected to each other by sharing three dicopper paddlewheel SBUs, and arranged in an alternating fashion along the crystallographic *c* axis (Fig. 1b). The spherical cage consists of 12 ligands and 6 SBUs, and the diameter is about 14 Å, taking into account the van der Waals radii of atoms, while the shuttle-shaped cage is constructed from 6 ligands and 12 SBUs. Compared to the parent MOF **ZJNU-50**, the shuttle-shaped cage in **ZJNU-53a** is dissected into three small ones due to the naphthalene ring pointing towards the cage (Fig. 1), which might help improving gas adsorption at high pressure. Note that Fig. 1 only represents one plausible way of the shuttle-shaped cage partition because the naphthalene ring and the triple bond are position disordered.

It should be mentioned that the naphthalene ring of the organic ligand is very difficult to identify solely from the crystallographic aspect due to the severe disorder and weak diffraction, although the diffraction data were collected at a low temperature of 120 K, and therefore some commands were employed to model the structure during the structure refinement. Furthermore, the chemical structure of the organic linker can be unambiguously confirmed by taking the ^{1}H NMR spectra of the acid-digested samples, which show that the organic linker remains intact during the solvothermal reaction (Fig. S8†). Also, PXRD data show a good agreement with the one simulated from this cif, validating the structural characterization.

The permanent porosity was evaluated by nitrogen adsorption measurements at 77 K using an ASAP 2020 HD88 equipment. Before any adsorption measurement, the as-synthesized MOF was activated by guest-exchange with dry acetone followed by evacuation under dynamic vacuum at 373 K. After activation, the framework is preserved as confirmed by powder X-ray diffraction studies. As shown in Fig. 2a, the activated MOF exhibited a Type-I isotherm, typical of microporous materials. The apparent Brunauer–Emmett–Teller (BET) surface area and pore volume were calculated to be 3034 m^2 g^{-1} and 1.084 cm^3 g^{-1}, respectively (Fig. S3†). These values are

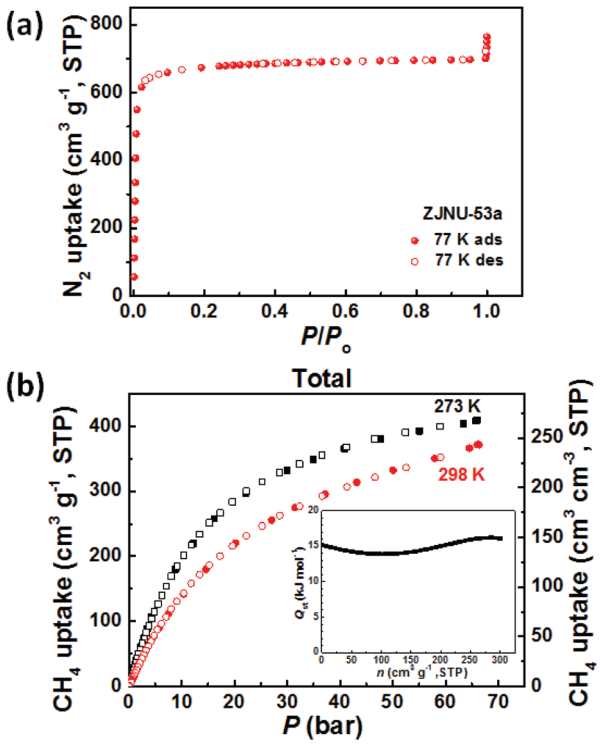

Fig. 2 (a) N_2 adsorption–desorption isotherms of **ZJNU-53a** at 77 K; (b) high-pressure methane adsorption isotherms at 273 and 298 K. Inset: isosteric heat of methane adsorption as a function of methane loadings. Solid and open symbols represent adsorption and desorption, respectively.

systematically lower than those of **ZJNU-50a** due to the naphthalene ring pointing towards the pore cage.

In light of such favourable porosities, high-pressure methane sorption measurements were performed at the Center for Neutron Research, National Institute of Standards and Technology (NIST) using a computer-controlled Sieverts apparatus. Fig. 2b shows the gravimetric and volumetric methane adsorption isotherms in **ZJNU-53a** at 273 K and 298 K for pressures up to 65 bar. It should be mentioned that the crystal density of 0.6549 g cm^{-3} was used to calculate the volumetric uptake serving as an idealized maximum storage capacity. From the temperature-dependent isotherms, we extracted the isosteric heat of methane adsorption using Clausius–Clapeyron equations. As shown in Fig. 2b inset, the isosteric heat of methane adsorption firstly drops slightly and then increases. The initial Q_{st} value is 15.02 kJ mol^{-1}, comparable to those in other MOFs with dicopper paddlewheels.[2n,8] The adsorption and desorption branches basically overlap with each other, suggesting that the adsorption process is reversible and the adsorbed methane can be fully recovered during the desorption process. Regarding total capacities, **ZJNU-53a** exhibits a gravimetric methane uptake of 0.206 g g^{-1} at 298 K and 35 bar, corresponding to a volumetric one of 188 cm^3 (STP) cm^{-3}. If the packing loss is not considered, the latter value surpasses the DOE's old target of 180 cm^3 (STP) cm^{-3} for methane storage at 35 bar and ambient temperature, and is comparable (Table 1) to and even higher than those of isoreticular Cu-based MOFs such as NOTT-102 (181 cm^3 (STP) cm^{-3}),[2n] NU-135 (187 cm^3 (STP) cm^{-3}),[9] PCN-14 (195 cm^3 (STP) cm^{-3}),[3b] ZJU-5 (190 cm^3 (STP) cm^{-3}),[7] UTSA-80 (192 cm^3 (STP) cm^{-3}),[6] and NJU-Bai14 (184 cm^3 (STP) cm^{-3} at 290 K and 35 bar),[10] but lower than those observed in HKUST-1 (227 cm^3 (STP) cm^{-3}),[3b] UTSA-76 (211 cm^3 (STP) cm^{-3})[3c] and NiMOF-74 (228 cm^3 (STP) cm^{-3}).[3b] When the pressure increases to 65 bar, the volumetric methane uptake reaches 241 cm^3 (STP) cm^{-3}, which is really quite high. In fact, the value is slightly below the DOE's recently revised methane storage target of 263 cm^3 (STP) cm^{-3} if the packing loss is ignored.[11] Under this condition, the density of methane stored at the micropore is 0.2432 g cm^{-3}, which is equivalent to the density of compressed methane at 298 K and 383 bar, and 58% of the density of liquid methane at 113 K and 1 bar.

Apart from its high methane storage capacities, **ZJNU-53a** also exhibits high methane deliverable capacities, which is defined as the difference between the amounts of methane stored at the maximum fill service pressure and the amount stored at the depletion pressure. Assuming a pressure swing from 35 bar to 5 bar, **ZJNU-53a** exhibits a deliverable capacity of 135 cm^3 (STP) cm^{-3} at 298 K, which increases to 190 cm^3 (STP) cm^{-3} if 5 and 65 bar are taken as specific lower and upper pressure limits. That is, a tank filled with **ZJNU-53a** can deliver 74% as much fuel as the CNG tank operating in the same lower pressure limit and 248 bar as the upper pressure limit, indicating **ZJNU-53a** as a potential material for methane delivery. The volumetric methane deliverable amount is comparable (Table 1) to or even better than those MOFs that show the most promise for deliverable methane storage: MOF-5 (182 cm^3 (STP) cm^{-3}),[1b,12] NU-111 (179 cm^3 (STP) cm^{-3}),[3b] NU-125 (183 cm^3 (STP) cm^{-3}),[3b] PCN-14 (157 cm^3 (STP) cm^{-3}),[3b] and UTSA-80 (174 cm^3 (STP) cm^{-3}).[6]

By comparison of the methane adsorption capacities of **ZJNU-53a** and **ZJNU-50a**, it can be seen that **ZJNU-53a** outperformed **ZJNU-50a** on the basis of both volumetric storage and

Table 1 Methane adsorption in reported MOFs

	Total uptake at 65 (35) bar		Working capacity[a]		
MOFs	cm^3 cm^{-3}	g g^{-1}	cm^3 cm^{-3}	g g^{-1}	Ref.
ZJNU-53	241 (188)	0.264 (0.206)	190	0.206	This work
ZJNU-50	229 (178)	0.274 (0.213)	184	0.220	4
UTSA-80	233 (192)	0.240 (0.198)	174	0.178	6
UTSA-76	257 (211)	0.263 (0.216)	197	0.201	3c
HKUST-1	267 (227)	0.216 (0.184)	190	0.154	3b
NiMOF-74	251 (228)	0.148 (0.135)	129	0.077	3b
PCN-14	230 (195)	0.197 (0.169)	157	0.136	3b
ZJU-5	228 (190)	0.240 (0.200)	168	0.177	7
NU-125	232 (182)	0.287 (0.225)	183	0.227	3b
NU-111	206 (138)	0.360 (0.241)	179	0.313	3b
NOTT-102	237 (181)	0.288 (0.220)	192	0.233	2n
MOF-5	214 (150)	0.246 (0.172)	182	0.209	1b

[a] The working capacity is defined as the difference in total uptake between 65 and 5 bar.

working capacities. As established before,[2n] the methane uptake of NbO-type MOFs at room temperature and 5 bar is mainly dominated by the primary adsorption sites such as the open copper sites and window sites, while at a high pressure of 65 bar, these strong adsorption sites would have been largely occupied and the secondary adsorption sites start to play a role. Based on this analysis, the improved methane storage and working capacities of **ZJNU-53a** should be attributed to the better secondary adsorption surface in the MOF **ZJNU-53a**, since the two isoreticular MOF materials have similar primary adsorption sites. The better secondary adsorption surface in the MOF **ZJNU-53a** should be originated from ligand modification, which leads to the small pore size and polarized pi-electron surface enhancing the interactions with methane molecules at higher loadings of methane.

In summary, by pore structure optimization, we achieved a NbO-type MOF **ZJNU-53a** exhibiting much higher volumetric methane storage and working capacities than the parent MOF **ZJNU-50a**. At 298 K and 65 bar, the volumetric methane storage and working capacities reach 241 and 190 cm^3 (STP) cm^{-3}, respectively, if the packing loss is not considered, which are among the highest reported for all MOFs. It is expected that this work will provide useful guidance for optimal design of MOF materials for methane storage.

This work was supported by the National Natural Science Foundation of China (no. 21301156) and the Qianjiang talents project in Zhejiang province (ZC304015017).

Notes and references

1 (*a*) Y. He, W. Zhou, G. Qian and B. Chen, *Chem. Soc. Rev.*, 2014, **43**, 5657–5678; (*b*) J. A. Mason, M. Veenstra and J. R. Long, *Chem. Sci.*, 2014, **5**, 32–51; (*c*) T. A. Makal, J.-R. Li, W. Lu and H.-C. Zhou, *Chem. Soc. Rev.*, 2012, **41**, 7761–7779; (*d*) K. Konstas, T. Osl, Y. Yang, M. Batten, N. Burke, A. J. Hill and M. R. Hilla, *J. Mater. Chem.*, 2012, **22**, 16698–16708; (*e*) W. Zhou, *Chem. Rec.*, 2010, **10**, 200–204.

2 (*a*) M. Kondo, T. Yoshitomi, K. Seki, H. Matsuzaka and S. Kitagawa, *Angew. Chem., Int. Ed. Engl.*, 1997, **36**, 1725–1727; (*b*) M. Eddaoudi, J. Kim, N. Rosi, D. Vodak, J. Wachter, M. O'Keeffe and O. M. Yaghi, *Science*, 2002, **295**, 469–472; (*c*) I. Senkovska and S. Kaskel, *Microporous Mesoporous Mater.*, 2008, **112**, 108–115; (*d*) P. L. Llewellyn, S. Bourrelly, C. Serre, A. Vimont, M. Daturi, L. Hamon, G. D. Weireld, J.-S. Chang, D.-Y. Hong, Y. K. Hwang, S. H. Jhung and G. Férey, *Langmuir*, 2008, **24**, 7245–7250; (*e*) H. Kim, D. G. Samsonenko, S. Das, G.-H. Kim, H.-S. Lee, D. N. Dybtsev, E. A. Berdonosova and K. Kim, *Chem. – Asian J.*, 2009, **4**, 886–891; (*f*) P. D. C. Dietzel, V. Besikiotis and R. Blom, *J. Mater. Chem.*, 2009, **19**, 7362–7370; (*g*) H. Wu, W. Zhou and T. Yildirim, *J. Am. Chem. Soc.*, 2009, **131**, 4995–5000; (*h*) D. Yuan, D. Zhao, D. Sun and H.-C. Zhou, *Angew. Chem., Int. Ed.*, 2010, **49**, 5357–5361; (*i*) D. Han, F.-L. Jiang, M.-Y. Wu, L. Chen, Q.-H. Chen and M.-C. Hong, *Chem. Commun.*, 2011, **47**, 9861–9863; (*j*) U. Stoeck, S. Krause, V. Bon, I. Senkovska and S. Kaskel, *Chem. Commun.*, 2012, **48**, 10841–10843; (*k*) D. Liu, H. Wu, S. Wang, Z. Xie, J. Li and W. Lin, *Chem. Sci.*, 2012, **3**, 3032–3037; (*l*) Q. Yang, V. Guillerm, F. Ragon, A. D. Wiersum, P. L. Llewellyn, C. Zhong, T. Devi, C. Serre and G. Maurin, *Chem. Commun.*, 2012, **48**, 9831–9833; (*m*) X. Zhao, D. Sun, S. Yuan, S. Feng, R. Cao, D. Yuan, S. Wang, J. Dou and D. Sun, *Inorg. Chem.*, 2012, **51**, 10350–10355; (*n*) Y. He, W. Zhou, T. Yildirim and B. Chen, *Energy Environ. Sci.*, 2013, **6**, 2735–2744; (*o*) D. A. Gomez-Gualdron, O. V. Gutov, V. Krungleviciute, B. Borah, J. E. Mondloch, J. T. Hupp, T. Yildirim, O. K. Farha and R. Q. Snurr, *Chem. Mater.*, 2014, **26**, 5632–5639.

3 (*a*) S. Ma, D. Sun, J. M. Simmons, C. D. Collier, D. Yuan and H.-C. Zhou, *J. Am. Chem. Soc.*, 2008, **130**, 1012–1016; (*b*) Y. Peng, V. Krungleviciute, I. Eryazici, J. T. Hupp, O. K. Farha and T. Yildirim, *J. Am. Chem. Soc.*, 2013, **135**, 11887–11894; (*c*) B. Li, H.-M. Wen, H. Wang, H. Wu, M. Tyagi, T. Yildirim, W. Zhou and B. Chen, *J. Am. Chem. Soc.*, 2014, **136**, 6207–6210; (*d*) F. Gándara, H. Furukawa, S. Lee and O. M. Yaghi, *J. Am. Chem. Soc.*, 2014, **136**, 5271–5274.

4 C. Song, Y. Ling, Y. Feng, W. Zhou, T. Yildirim and Y. He, *Chem. Commun.*, 2015, **51**, 8508–8511.

5 (*a*) M. Li, D. Li, M. O'Keeffe and O. M. Yaghi, *Chem. Rev.*, 2014, **114**, 1343–1370; (*b*) Y. He, B. Li, M. O'Keeffe and B. Chen, *Chem. Soc. Rev.*, 2014, **43**, 5618–5656.

6 H.-M. Wen, B. Li, D. Yuan, H. Wang, T. Yildirim, W. Zhou and B. Chen, *J. Mater. Chem. A*, 2014, **2**, 11516–11522.

7 X. Rao, J. Cai, J. Yu, Y. He, C. Wu, W. Zhou, T. Yildirim, B. Chen and G. Qian, *Chem. Commun.*, 2013, **49**, 6719–6721.

8 Y. Peng, G. Srinivas, C. E. Wilmer, I. Eryazici, R. Q. Snurr, J. T. Hupp, T. Yildirim and O. K. Farha, *Chem. Commun.*, 2013, **49**, 2992–2994.

9 R. D. Kennedy, V. Krungleviciute, D. J. Clingerman, J. E. Mondloch, Y. Peng, C. E. Wilmer, A. A. Sarjeant, R. Q. Snurr, J. T. Hupp, T. Yildirim, O. K. Farha and C. A. Mirkin, *Chem. Mater.*, 2013, **25**, 3539–3543.

10 M. Zhang, Q. Wang, Z. Lu, H. Liu, W. Liu and J. Bai, *CrystEngComm*, 2014, **16**, 6287–6290.

11 See the DOE MOVE program at https://arpa-e-foa.energy.gov/.

12 H. Furukawa, N. Ko, Y. B. Go, N. Aratani, S. B. Choi, E. Choi, A. Ö. Yazaydin, R. Q. Snurr, M. O'Keeffe, J. Kim and O. M. Yaghi, *Science*, 2010, **329**, 424–428.

